Published by :
http://www.ijert.org

International Journal of Engineering Research & Technology (IJERT)
ISSN: 2278-0181
Vol. 12 Issue 08, August-2023

Design and Analysis of Skateboard Electric Vehicle chassis and Battery Pack

Shashank.N [1]
Department of Mechanical Engineering
RV College of Engineering
Bangalore, India

Shashank.P [2], Gopalakrishna. HD [3]
Department of Mechanical Engineering
RV College of Engineering
Bangalore, India

***Abstract* - This paper presents a comprehensive study of the skateboard electric vehicle chassis. It discusses the key design considerations for skateboard electric vehicle chassis, such as weight distribution, and structural integrity. The focus is to achieve greater factor of safety in all the loading conditions, manly designed for strength. The battery analysis is mainly focused on structural integrity as well as the frequency response with other parameters including natural frequency of the chassis to avoid resonance.**

Keywords - FEA; Skateboard Chassis; MATLAB; Vehicle Dynamics;

I. INTRODUCTION

The skateboard electric vehicle chassis, a pivotal component within the realm of electric mobility, has fundamentally reshaped the landscape of urban transportation. As electric vehicles have gained prominence, the skateboard chassis has emerged as a crucial structural foundation for small electric vehicles like electric skateboards. This paper offers an all-encompassing exploration of this innovative chassis, spanning its historical progression, intricate design considerations, material selection, performance implications, and its profound influence on user experience [1]. With the evolution of electric skateboard chassis tracing back to their inception, the transition from conventional wooden decks to modular designs capable of accommodating intricate electric components signifies a transformative shift [2]. Key design aspects, including weight distribution, aerodynamics, and structural integrity, are meticulously balanced to optimize vehicle dynamics. As technology advances, the chassis is poised to evolve further, with anticipated integration of AI-driven controls, advanced battery systems, and heightened connectivity [3]. In summation, the skateboard electric vehicle chassis stands as a testament to sustainable urban mobility innovation, encapsulating a rich history, intricate engineering, and a promising future. Conventional vehicle chassis, prevalent in traditional automobiles, typically follow a frame-based structure, encompassing the engine, drivetrain, suspension, and body components [4,7]. This arrangement prioritizes passenger comfort and safety within a complex framework. In contrast, skateboard vehicle chassis, notably employed in electric skateboards and compact electric vehicles, embrace a more streamlined and modular approach [8,9]. These chassis designs integrate essential components like motors, batteries, and control systems into a single platform, often resembling a skateboard deck. A battery case, referred to as a battery enclosure or battery housing, serves as a safeguarding and enclosing framework meticulously created to envelop individual or multiple battery cells [10]. The principal function of a battery case revolves around furnishing a stable and secure milieu for these cells. Its purpose spans the prevention of external physical harm and guarding the cells against environmental elements like moisture, dust, and pollutants, all of which could potentially compromise battery efficiency and longevity [11]. Furthermore, the case acts as a protective barricade, effectively mitigating potential thermal incidents and lowering the susceptibility to thermal runaway or fire hazards[12, 13]. However, in this research paper a MATLAB GUI (Graphical User Interface) is developed to calculate vehicle dynamics of the car, a structural analysis, modal analysis is carried out using Finite Element Analysis (FEA) and structural analysis of battery pack as well as the harmonic frequency response

II. COMPUTING VEHICLE DYNAMIC FORCES

A. Longitudinal Normal Forces on Inclined Surface

Longitudinal normal forces on an inclined surface refer to the perpendicular forces that act between an object and the inclined plane due to their contact. These forces are oriented perpendicular to the surface and are distinct from the gravitational force as shown in Figure 1.

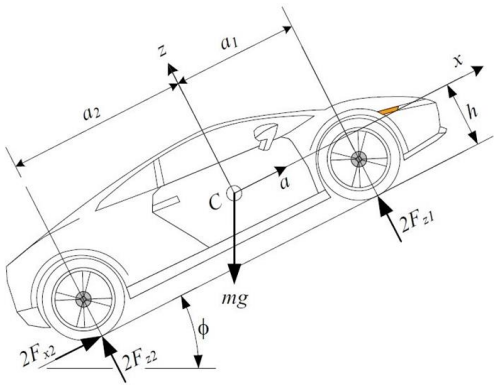

International Journal of Engineering Research & Technology (IJERT)
ISSN: 2278-0181
Vol. 12 Issue 08, August-2023

Figure 1: Free Body Diagram for Inclined Surface [1]

The equations (1) and (2) offer insights into the reaction forces and brake forces applicable to both the vehicle's rear and front wheels.

$$Fz_1 = ((0.5 \times m \times g \times a_2/l \times \cos(\emptyset)) - (0.5 \times h_g/l \times \sin(\emptyset))) \quad (1)$$

$$Fz_2 = ((0.5 \times m \times g \times a_1/l \times \cos(\emptyset)) - (0.5 \times h_g/l \times \sin(\emptyset))) \quad (2)$$

Where,

Fx_2 & Fx_1: Overall traction or brake force under rear wheels and front wheels

m : Mass of the car

$\emptyset$: Road angle

a_2 : Distance of Rear axle from mass center

a_1 : Distance of Front axle from mass center

B. *Lateral Normal Forces on Banked Surface*

Lateral normal forces on a banked surface pertain to the perpendicular forces exerted between an object and the inclined, banked plane due to their contact. These forces act perpendicular to the surface and are distinct from gravitational forces. They are essential in maintaining the object's trajectory and preventing it from sliding down the banked surface, particularly in scenarios involving vehicles on curved roads or tracks as shown in Figure 2. The equations (3) and (4) offer insights into the reaction forces and brake forces applicable to both the vehicle's upper and lower wheels.

$$Fz_1 = ((0.5 \times m \times g \times b_2/w \times \cos(\emptyset)) - (0.5 \times h_g/w \times \sin(\emptyset))) \quad (3)$$

$$Fz_1 = ((0.5 \times m \times g \times b_1/w \times \cos(\emptyset)) - (0.5 \times h_g/w \times \sin(\emptyset))) \quad (4)$$

Where,

w : Track Width

b_2: Distance of right wheels from mass center

b_1: Distance of left wheels from mass center

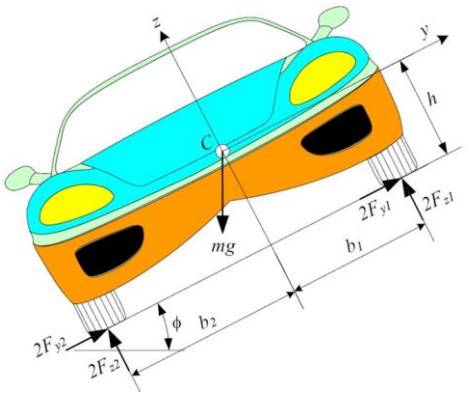

Figure 2: Normal force under banking condition [1]

C. *Computing force acting on the vehicle using developed MATLAB Calculator and validation*

Utilizing a collection of equations from the Design Input section, a Graphical User Interface (GUI) Calculator was developed in MATLAB. This calculator facilitates the extraction of vehicle dynamic parameters, illustrated in Figures 3 and 4. The rationale behind this tool's creation was to eradicate the requirement for intricate calculations across diverse load situations, streamlining the process for various load scenarios. This validation involved cross-referencing the calculator's outputs with manually computed values and benchmarking using equations (6). The rigorous validation process assures users of the calculator's precision and affirms its utility in delivering efficient and accurate vehicle dynamics insights across diverse scenarios.

$$F_{total} = F_{rolling} + F_{gradient\ resistance} + F_{acceleration} + F_{aerodynamic\ drag} \quad (6)$$

Substituting values to get necessary total friction to overcome for the vehicle to move,

$$F_{total} = \mu mg\cos(\alpha) + m \times g \times \sin(\alpha) + 0.5 \times m_w \times r^2 \times a \times m + 0.5 \times C_A \times A_f \times \rho \times V^2 \quad (7)$$

F_{total}=0.011×900×9.81×cos(0)+900×9.81×sin(0)+0.5×40×0.6× 0.6× 0.65× 900+0.5× 0.275× 1.3× 1.5× 1.2× 25× 25

F_{total}= 4514.40 Newton

W_{front}=(L_b/L)×(M×g×cos(α))-(hg/L)×(F_{total}-$F_{rolling}$×(1-(r_{dyn}/h_g)) (8)

W_{rear} =(La/L)×(M×g×cos(α))+(hg/L)*(F_{total}-$F_{rolling}$×(1-(r_{dyn}/hg)) (9). After substituting we get,

W_{front}=(0.85/1.75)×(900×9.81×cos(0))-(0.4/1.75)×(4514.40-97.118×(1-(0.35/0.4))

Wrear=(0.85/1.75)×(900×9.81×cos(0))-(0.3/1.75)×(4514.40-97.118×(1-(0.35/0.3))

W_{front} = 3259.28 Newton and W_{rear} = 5317.46 Newton

Similarly computing equations (1,2,3 and 4) manually we get,

F_{z1} = 2077.32 Newton – Longitudinal Front Axle Normal Force
F_{z2} = 2211.04 Newton – Longitudinal Rear Axle Normal Force
F_{z1} = 2207.25 Newton – Lateral Upper Side Normal Force
F_{z2} = 2207.25 Newton – Lateral Lower Side Normal Force
Manual calculations align with MATLAB GUI results.

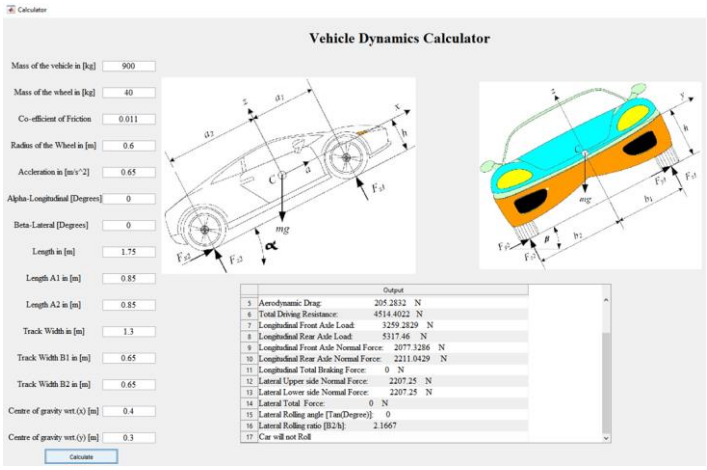

Figure 3: MATLAB GUI Calculator

Published by :
http://www.ijert.org

International Journal of Engineering Research & Technology (IJERT)
ISSN: 2278-0181
Vol. 12 Issue 08, August-2023

	Output	
1	Rolling Resistance:	97.119 N
2	Gradient Resistance:	0 N
3	Road Resistance:	97.119 N
4	Acceleration Resistance:	4212 N
5	Aerodynamic Drag:	205.2832 N
6	Total Driving Resistance:	4514.4022 N
7	Longitudinal Front Axle Load:	3355.1442 N
8	Longitudinal Rear Axle Load:	5473.8558 N
9	Longitudinal Front Axle Normal Force:	2138.4265 N
10	Longitudinal Rear Axle Normal Force:	2276.0735 N
11	Longitudinal Total Braking Force:	0 N
12	Lateral Upper side Normal Force:	2207.25 N
13	Lateral Lower side Normal Force:	2207.25 N

Figure 4: Result Window

III. DESIGN & MODELLING

The conceptual design phase represents the inception of the design journey, encompassing the earliest stage in the process. Its fundamental objective is to delineate the envisioned product by weaving together a cohesive array of ideas and concepts. These concepts not only elucidate the product's intended functionality but also encapsulate its visual attributes, all presented in a manner that resonates with user understanding.

Finally, by unwaveringly retaining the core attributes of the skateboard chassis and systematically addressing the concerns highlighted in the prior iterations, a notable solution surfaced. This encompassed a perceptive reduction in the count of joints by an impressive 50%, symbolizing a shift to integrating two joints within each swing arm. As a result, the overall implementation of the chassis witnessed a streamlined total of eight joints. To counter the potential impact of external forces leading to torsional stress, a well-thought-out H-configuration was strategically introduced at the center. This inventive inclusion not only thwarted chassis twisting under torsional loads but also showcased a seamless amalgamation of inventive issue-solving with pragmatic engineering, as shown in Figure 5. Which is modeled using SolidWorks.

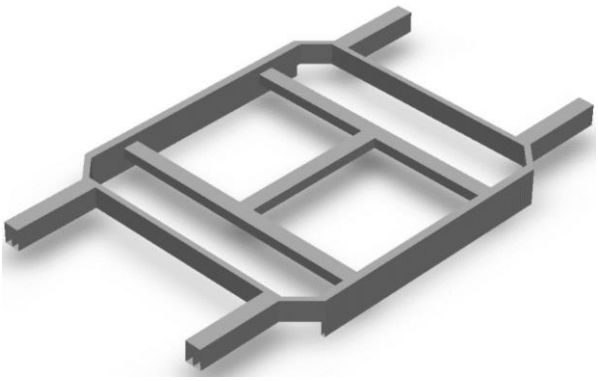

Figure 5: 3D Model of Skateboard Chassis

A. *Preliminary Design of Skateboard Chassis*

During the preliminary design phase, the primary aim is to establish the rough dimensions and pertinent physical attributes of the subject at hand. The deliberations undertaken in this phase aim to enhance the optimization of the conceptual design. Subsequently, the conceptual design will undergo further refinement to incorporate additional intricacies into the overall design.

B. *Selection of Material*

Table 1 Aluminium ISO 6061-T6 Property

Yield Stress (MPa)	Poisson's Ratio	Density kg/mm^3
276	0.33	2.7 x 10^{-6}

The selection of materials carries substantial significance within the context of the skateboard chassis platform, primarily due to its role in enabling the creation of diverse body-in-white structures. In light of this, the chassis design places a premium on prioritizing strength over stiffness. This strategic approach ensures the establishment of a resilient chassis configuration, thereby enhancing security measures and elevating the overall safety quotient. This deliberate focus on safety not only opens avenues for the exploration and advancement of a wide array of body-in-white designs but also drives the choice of materials. The selection process hinges on the criteria of high yield strength and ample availability, essential for large-scale chassis manufacturing. The grade IS 65028-T6, or ISO 6061-T6, distinguished by a yield strength of 276 MPa, emerges as the fitting choice due to its optimal yield strength attributes. Detailed mechanical properties of ISO 6061-T6 can be found in Table 1.

C. *Selection of Section based on BIS Standard*

The skateboard chassis incorporating four distinct cross-sectional profiles for its primary members, cross members, and extended suspension support arms, the choice of these profiles revolves around the goal of maximizing the moment of inertia while adhering to an equivalent cross-sectional area. This optimization procedure is seamlessly facilitated through a specialized MATLAB calculator, meticulously designed for conducting the requisite computations, as shown in Figure 6.

Within the array of available cross-sectional choices, both the rectangular and square sections demonstrate the most elevated moment of inertia. Consequently, a fusion of these two cross-sectional profiles yields the highest moment of inertia when compared to the alternative C-section. Aligning with the chart furnished by the BIS standard, which outlines commercially accessible sizes, the chassis showcases distinctive cross-sectional designs, as illustrated in Figure 7.

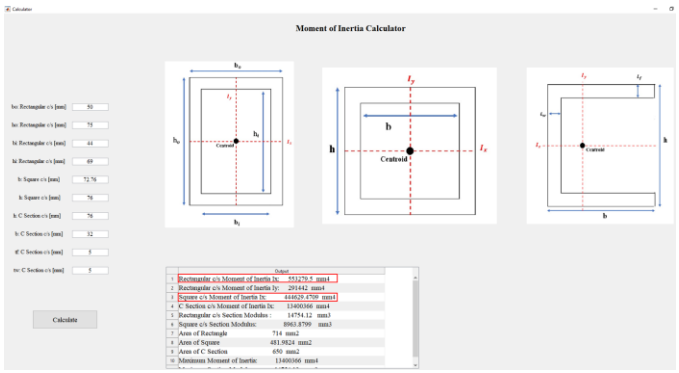

Figure 6: Moment of Inertial Calculator

International Journal of Engineering Research & Technology (IJERT)
ISSN: 2278-0181
Vol. 12 Issue 08, August-2023

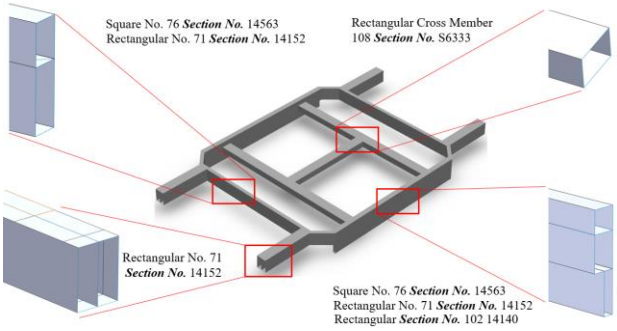

Figure 7: Cross Section of Chassis based on BIS Standard

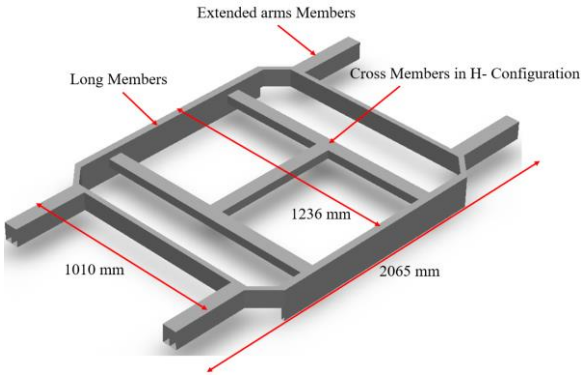

Figure 8: Refined Skateboard Chassis 3D Model

D. *Refined Design of Skateboard Chassis*

The platform model, a product of the conceptual design, has been subject to thorough and careful refinement. This intricate process took into account the designated material and cross-sectional area criteria, guided by the stipulations set forth in the BIS Standards, as exemplified in Figure 8 The process of enhancing the chassis was effectively conducted through the utilization of SolidWorks modeling software.

IV. Finite Element Analysis

FEA involves the simulation of diverse physical phenomena through the utilization of the numerical methodology known as the finite element method (FEM). This approach serves as a valuable tool for engineers, mitigating the need for extensive physical prototypes and experiments. Through FEA, engineers can refine component designs during the developmental phase, leading to enhanced products and improved outcomes.

A. *Element Geometries*

With a wide selection of commercially accessible software at hand, the analysis is executed utilizing the ANSYS Mechanical APDL FEA package. This inclusive package encompasses an assortment of elements, each designed to suit specific applications, effectively addressing diverse analysis demands. The specific elements employed in this context can be found in Table 2.

Sr. No.	Component	Element
1.	Long Members, Extended Members and Cross Members	SHELL element - 3D nodes 181
2.	Mass of the Battery Pack	Structural mass -3D mass 21

B. *Meshing*

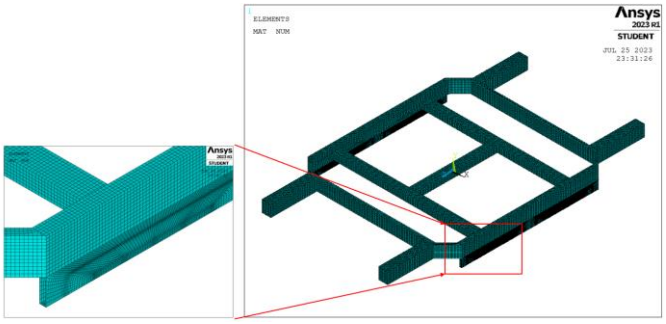

Figure 9: Fine Meshes Chassis

Meshing is a critical procedure integral to the realm of FEA. This operation involves the division of geometry into multiple smaller units known as elements. The precision and duration of the analysis are influenced by factors such as mesh size and the total count of elements. To ensure refined accuracy of outcomes, the application of Mesh Convergence is introduced. In this specific analysis, a mesh size of 10 is selected. Notably, Sections No. 76 and 71 feature a mesh size of 10mm, Section No. 102 employs a mesh size of 5mm, while Section No. 108 maintains a mesh size of 10mm. Given the geometry's linear nature, quadrilateral elements are chosen. Furthermore, SHELL elements are applied to Long Members, Extended Members, and Cross Members. To replicate the masses at their respective centers of gravity, the Structural MASS - 3D mass 21 element is deployed. This methodology is also extended to the mass determination of the Battery Pack as shown in Figure 9.

C. *Vehicle Parked on Level Road*

The static analysis incorporates both the inherent weight of the car chassis and an applied payload of 6867 N in the negative Y-axis direction. This payload is influenced by the gravitational acceleration aligned along the negative Y-axis of the plane, alongside a normal force of 2427 N. The chassis's front member is constrained with Ux=Uy=Uz=0, permitting rotational movement in the three remaining directions, as depicted in Figures 10 and 11.

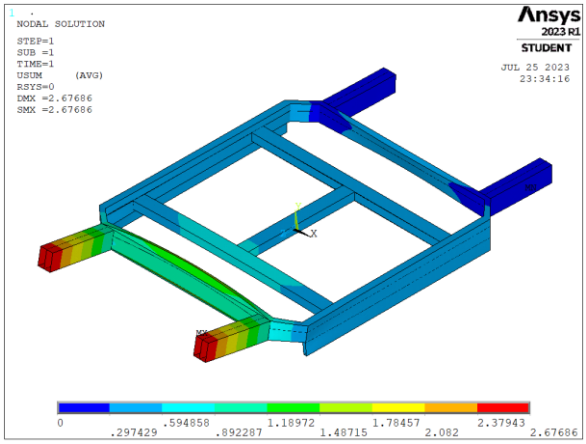

Figure 10: Defection Plot

International Journal of Engineering Research & Technology (IJERT)
ISSN: 2278-0181
Vol. 12 Issue 08, August-2023

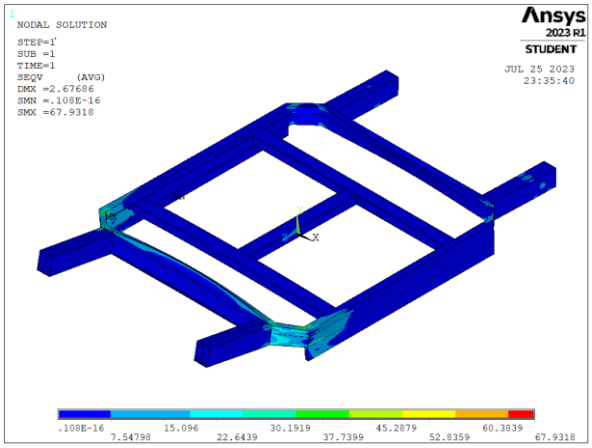

Figure 11: Stress Plot

D. Longitudinal Condition Vehicle Parked on Inclined Road

Operating under a longitudinal inclination of 24 degrees, the vehicle's arrangement is defined. In this particular configuration, the static analysis encompasses the intrinsic weight of the chassis, supplemented by a negative Y-axis applied payload of 6867 N, alongside a positive Y-axis normal force of 3000 N. The gravitational acceleration is oriented along the negative Y-axis. By imposing Ux=Uy=Uz=0 constraints on the front chassis member, rotational motion is facilitated in the three remaining directions as shown in Figure 12.

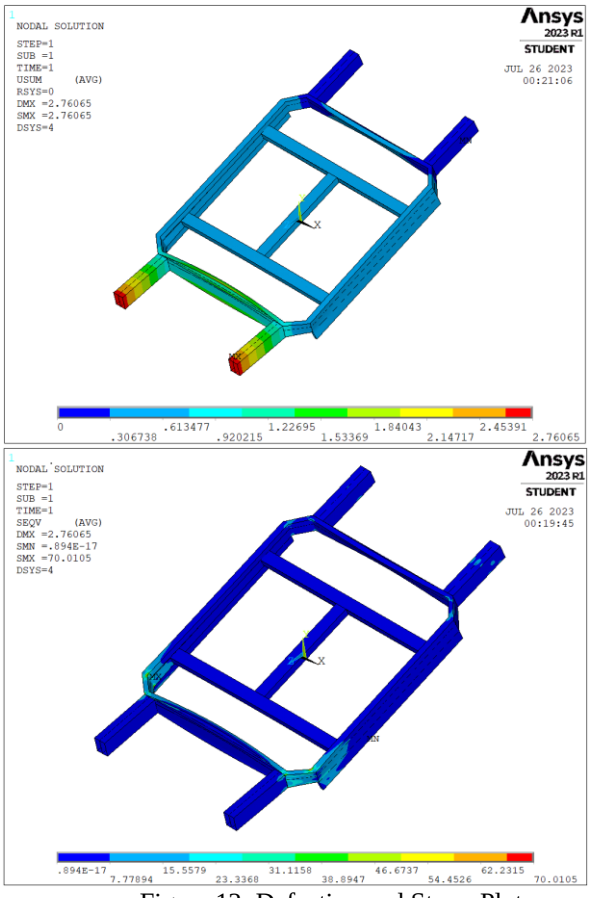

Figure 12: Defection and Stress Plot

E. Lateral Condition Vehicle Parked on Inclined Road

The vehicle is positioned at a lateral inclination of 24 degrees. In this particular setup, the static analysis encompasses the chassis's intrinsic weight, accompanied by an applied payload of 6867 N in the negative Y-axis direction. This load is subjected to the gravitational acceleration aligned with the negative Y-axis of the plane, alongside a normal force of 2091.6 N. Constraints of Ux=Uy=Uz=0 is imposed on the upper tire member of the chassis, enabling rotational mobility in the three remaining directions, as shown in the Figure 13.

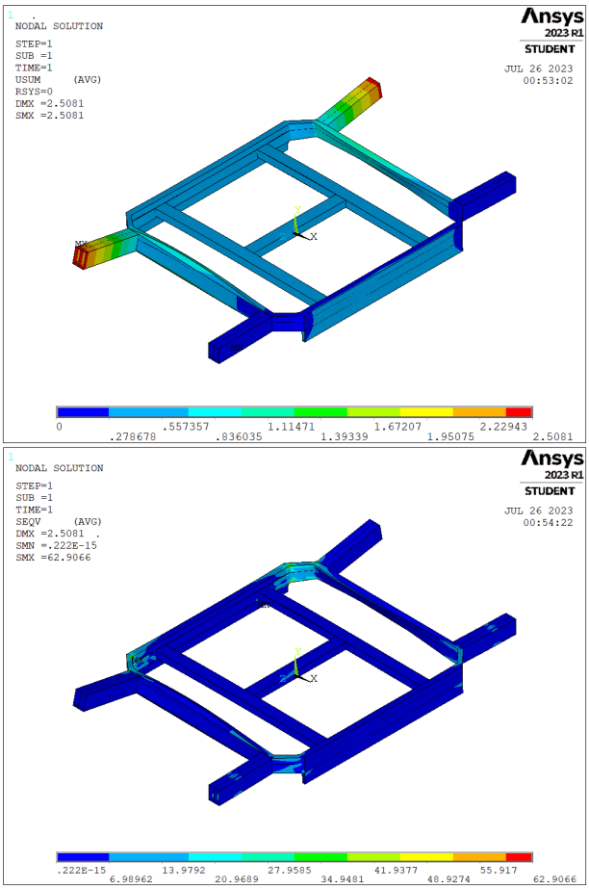

Figure 13: Defection and Stress Plot

F. Acceleration Condition along Transverse Condition / Cornering Condition

The vehicle experiences cornering with an acceleration reaching up to 3g. Within this specific configuration, the static analysis encompasses both the inherent weight of the chassis and an applied payload of 6867 N directed along the negative Y-axis. This load is affected by the gravitational acceleration aligned with the plane's negative Y-axis, complemented by a normal force of 2427 N. Applying constraints of Ux=Uy=Uz=0 to the front and rear chassis members, the chassis gains the capacity for rotational movement in the three remaining directions. These specific arrangements are visually shown in Figure 14.

International Journal of Engineering Research & Technology (IJERT)
ISSN: 2278-0181
Vol. 12 Issue 08, August-2023

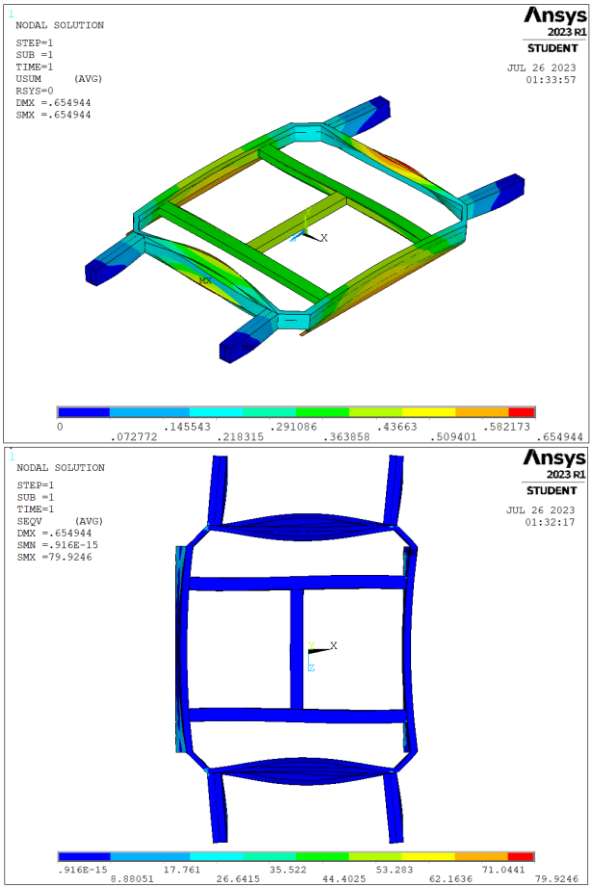

Figure 14: Defection and Stress Plot

G. *Acceleration Condition along Vertical Condition / vehicle subjected to sudden road bumps*

The vehicle is exposed to abrupt road disturbances of up to 2.5g. Within this specific arrangement, the static analysis incorporates both the inherent chassis weight and an applied payload of 6867 N, oriented in the negative Y-axis direction. This load is influenced by the gravitational acceleration aligned with the negative Y-axis of the plane, coupled with a normal force of 2427 N. Conforming to constraints of Ux=Uy=Uz=0, both the front and rear chassis members grant the chassis rotational flexibility in the remaining three directions. These configurations are visually illustrated in the accompanying Figure 15 and 16.

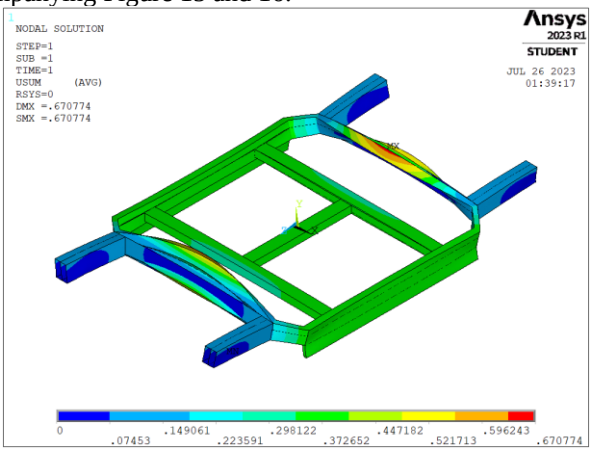

Figure 15: Defection Plot

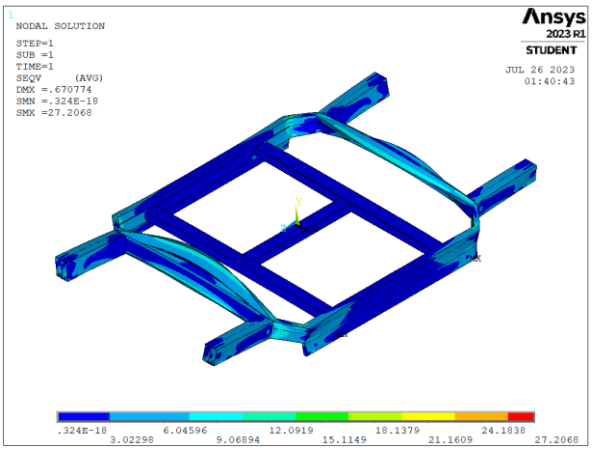

Figure 16: Stress Plot

H. *Acceleration Condition along Longitudinal Condition*

The vehicle accelerates on the road, reaching up to 2g. Within this specific arrangement, the static analysis incorporates both the inherent weight of the chassis and an applied payload of 6867 N directed along the negative Y-axis. This load is influenced by the gravitational acceleration aligned with the plane's negative Y-axis, complemented by a normal force of 2427 N. With the front and rear chassis members constrained by Ux=Uy=Uz=0, the chassis is enabled with rotational flexibility in the three remaining directions. These specific configurations are visually presented in the accompanying Figure 17.

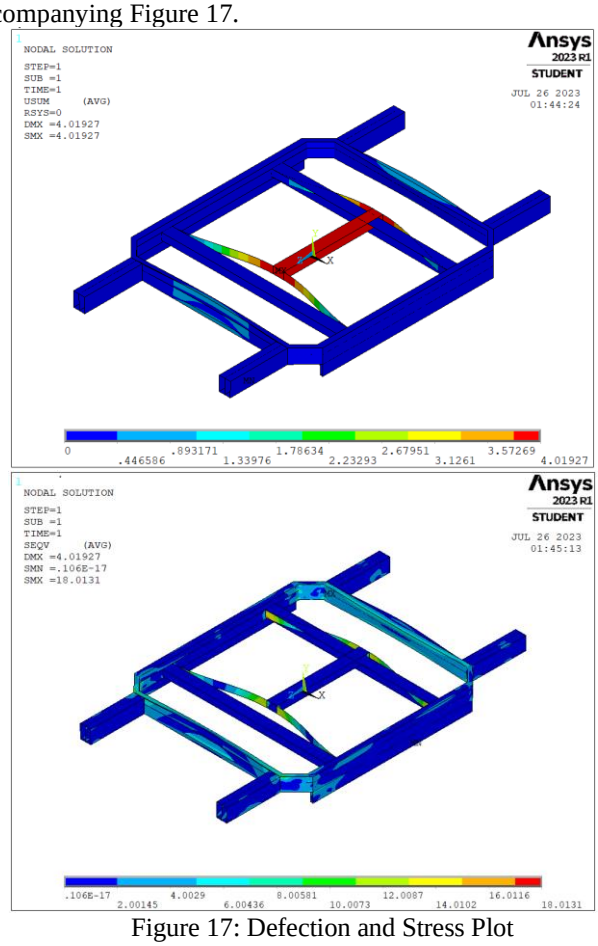

Figure 17: Defection and Stress Plot

International Journal of Engineering Research & Technology (IJERT)
ISSN: 2278-0181
Vol. 12 Issue 08, August-2023

I. Modal Analysis

Within this particular setup, the chassis's inherent weight is factored in by applying gravitational acceleration that aligns with the negative Y-axis of the plane. Both the front and rear chassis members are subjected to constraints covering all Degrees Of Freedom (DOF). These arrangements are visually represented in Figures 18.

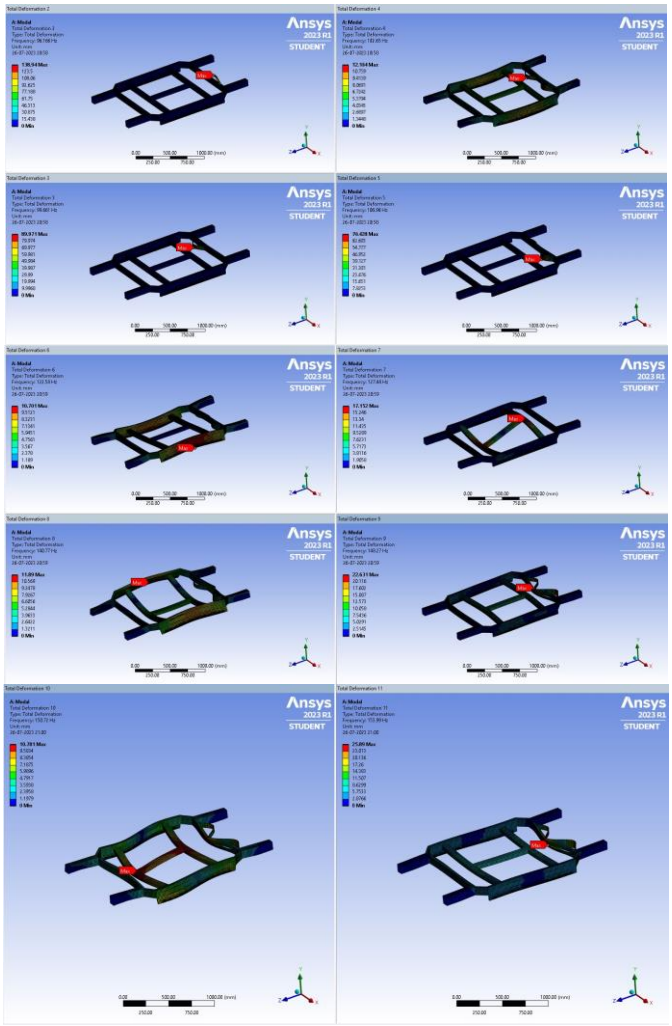

Figure 18: 10 Mode Shapes

J. Battery Pack Self Weight Condition

A comprehensive self-weight analysis was undertaken to assess structural integrity and load-bearing capacity. To emulate real-world conditions, the battery case mountings were constrained across all DOF, ensuring accurate representation of the system's response. As part of the analysis, a force of 490.5 N was precisely applied to the underside of the base plate, directed in the negative Y-axis direction. This meticulous simulation allowed for a detailed examination of the battery pack's ability to withstand both its intrinsic weight and external forces, yielding valuable insights into its mechanical behavior and potential stress distribution as shown in Figure 19 and 20.

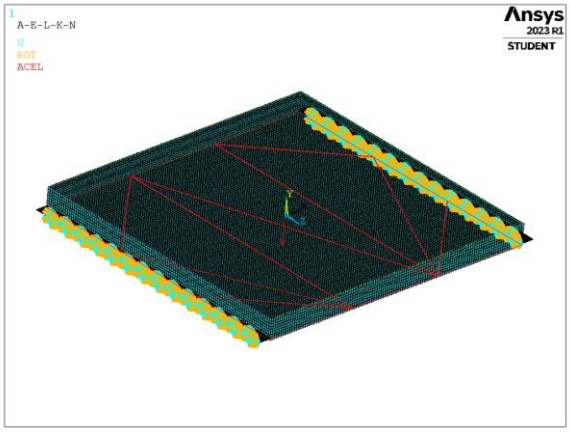

Figure 19: Boundary Condition of Battery Pack

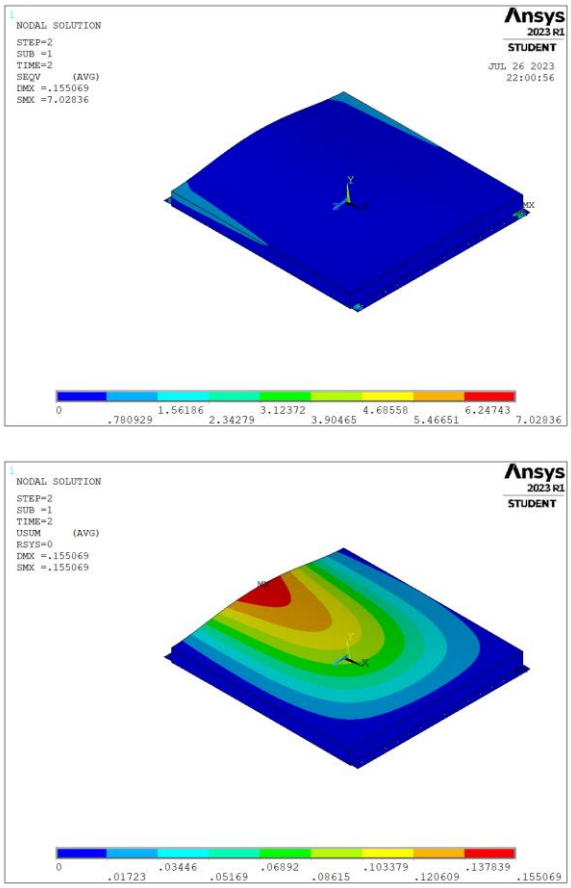

Figure 20: Stress and Deflection of Battery Pack

K. Harmonic Analysis of Battery Pack

A harmonic analysis of the battery pack is carried out in accordance with the AIS 048: 2009/AIS 156: 2019 standards is an integral step in ensuring compliance and optimal performance. This analysis involves a systematic investigation into the frequency components present in the electrical system, evaluating their potential impact on the battery pack's functionality and overall safety, as shown in Figures 21 and 22. By adhering to these standards, which outline specific guidelines and limits for harmonics, the assessment enables the identification and mitigation of undesirable harmonic distortions that might arise during operation.

Published by :
http://www.ijert.org

International Journal of Engineering Research & Technology (IJERT)
ISSN: 2278-0181
Vol. 12 Issue 08, August-2023

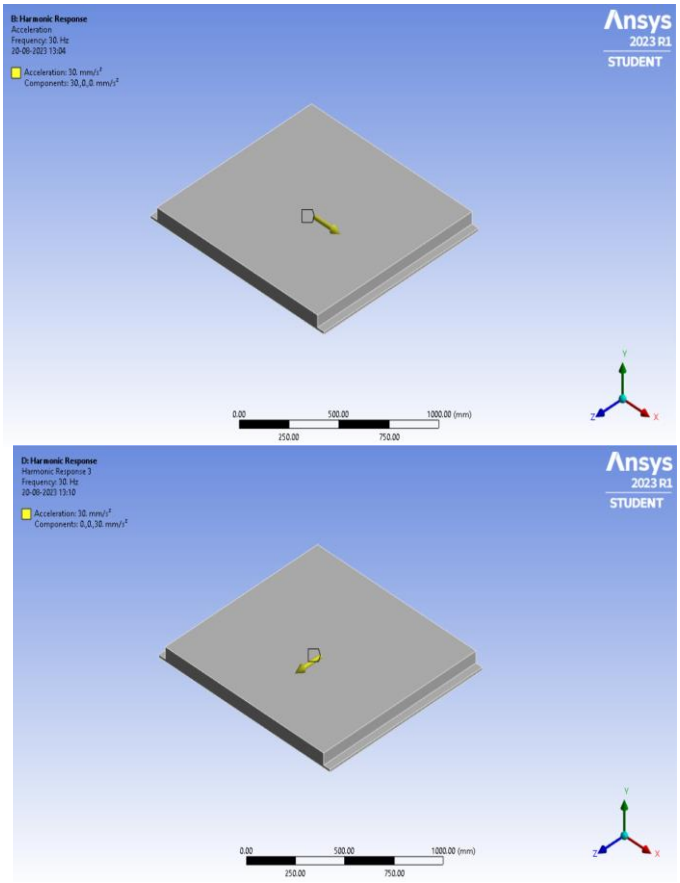

Figure 21: Harmonic Frequency Response in x and z direction

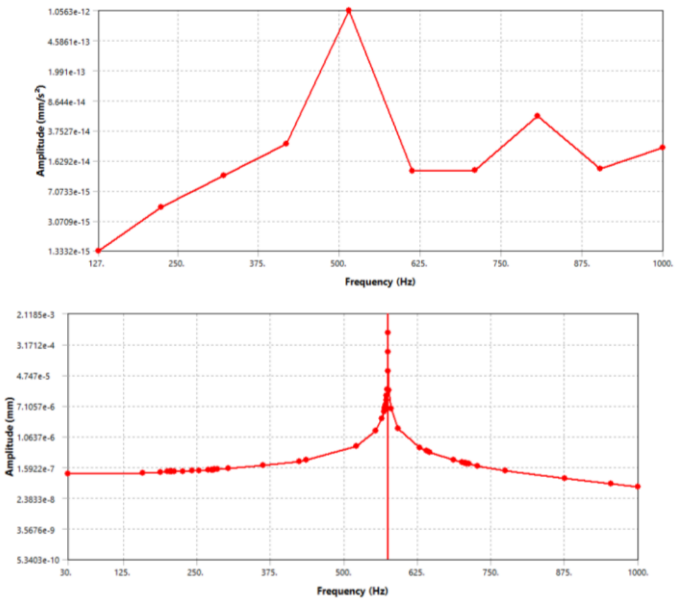

Figure 22: Frequency Response in x and z direction

V. RESULTS AND DISCUSSIONS

By taking into account all the specified load conditions, we can deduce the outcomes from the provided Table 3.

Table 3 Results

Load Cases	Stress	Deformation	FOS
1	67.96 N/mm^2	2.67 mm	4
2	70 N/mm^2	2.76 mm	3.9
3	62.9 N/mm^2	2.50 mm	4.3
4	79.92 N/mm^2	0.65 mm	3.4
5	27.2N/mm^2	0.67 mm	10.14
6	18 N/mm^2	4 mm	15.3

The powertrain operates within a working frequency range spanning from 30 to 70 Hz, contingent upon the motor capacity that varies between 3 kW and 10 kW. Based on the derived natural frequency, it can be inferred that resonance does not occur in relation to the operational frequencies of the motors as shown in Table 4.

Table 4 natural Frequency

Mode	Frequency
1.	85.81
2.	96.16
3.	99.66
4.	102.65
5.	106.96
6.	122.54
7.	127.44
8.	140.77
9.	148.27
10.	150.72

The self-weight analysis of the battery pack revealed a stress value of 7.02836 MPa and a deformation value of 0.155069. These findings were obtained from a comprehensive assessment involving 85124 meshed elements. The total mass of the battery pack was determined to be 93 kg. These results shed light on the structural response and load-bearing capacity of the pack under its intrinsic weight.

In terms of harmonic analysis, investigations were conducted along both the x and z directions. The analysis in the x direction exhibited a maximum amplitude of 1.1629e-12 mm at a resonating frequency of 515 Hz. Similarly, the analysis in the z direction showcased a maximum amplitude of 1.0563e-12 mm, also resonating at a frequency of 515 Hz. These outcomes underscore the importance of harmonic analysis in identifying deformations occurring at resonant frequencies, which could potentially impact the performance and reliability of the battery pack.

VI. CONCLUSION

Considering all the load scenarios, it can be concluded that the skateboard chassis possesses robust strength characteristics accompanied by a substantial factor of safety. Consequently, it becomes suitable not only for supporting passengers but also for accommodating diverse body-in-white structures. This extension paves the way for innovative concepts and designs for a wide range of vehicles beyond traditional passenger transport. Finite Element Analysis (FEA) conducted on the battery pack has yielded significant insights into its structural

International Journal of Engineering Research & Technology (IJERT)
ISSN: 2278-0181
Vol. 12 Issue 08, August-2023

behaviour and dynamic response. the self-weight analysis has yielded significant insights into its structural behaviour as it can withstand the minimum load i.e., its self-weight and has a deformation of 0.155069mm with a stress of 7.02836 MPa. Furthermore, the harmonic analysis performed in both the x and z directions has uncovered resonance phenomena within the system. the response, provides information about the cyclic deformation as a result of vibration on excited frequencies which helps to determine the maximum deformation at resonating frequency from Table 4, we can infer there is no resonance with respect to analyzed frequency response.

REFERENCES

[1] Thompson, Lonny L., Srikanth Raju, and E. Harry Law. "Design of a winston cup chassis for torsional stiffness." SAE transactions (1998): 2571-2584.

[2] Rodrigues, A. F. A., L. C. Gertz, A. Cervieri, A. L. R. Poncio, A. B. Oliveira, and M. S. Pereira. Static and dynamic analysis of a chassis of a prototype car. No. 2015-36-0353. SAE Technical Paper, 2015.

[3] Thompson, Lonny L., Jon K. Lampert, and E. Harry Law. Design of a twist fixture to measure the torsional stiffness of a winston cup chassis. No. 983054. SAE Technical Paper, 1998.

[4]] Sriram, N., D. Praveen Chandar, V. Arvind Subramanian, and M. Ganesh. "Design opportunities in electric skateboard." In 2017 International Conference on Intelligent Computing, Instrumentation and Control Technologies (ICICICT), pp. 1075-1078. IEEE, 2017.

[5] Roper, Stephen William Knox, and Il Yong Kim. "Integrated topology and packaging optimization for conceptual-level electric vehicle chassis design via the component-existence method." Proceedings of the Institution of Mechanical Engineers, Part D: Journal of Automobile Engineering (2022): 09544070221113895.,

[6] Mi, Tian, Gabor Stepan, Denes Takacs, Nan Chen, and Ning Zhang. "Model establishment and parameter analysis on shimmy of electric vehicle with independent suspensions." Procedia IUTAM 22 (2017): 259-266.

[7] Zhao, Yuqin, Fan Feng, and Runsheng Zhang. "Development of a four wheel independent drive and four wheel independent steer electric vehicle." In 2015 Sixth International Conference on Intelligent Systems Design and Engineering Applications (ISDEA), pp. 319-322. IEEE, 2015.

[8] Kurdi, Ojo, Ismoyo Haryanto, Gunawan Dwi Haryadi, and M. Wildan. "Dynamic analysis of electric bus chassis using finite element method." In 2018 5th International Conference on Electric Vehicular Technology (ICEVT), pp. 214-217. IEEE, 2018.

[9] Krishna, K., Mahesha, G.T., Hegde, S. and Satish Shenoy, B., 2023. A Review on Vibrations in Electric and Hybrid Electric Vehicles. Journal of The Institution of Engineers (India): Series C, 104(2), pp.423-438.

[10] De Sutter, L., Berckmans, G., Marinaro, M., Wohlfahrt-Mehrens, M., Berecibar, M. and Van Mierlo, J., 2020. Mechanical behavior of Silicon-Graphite pouch cells under external compressive load: Implications and opportunities for battery pack design. Journal of Power Sources, 451, p.227774.

[11] Peabody, C. and Arnold, C.B., 2011. The role of mechanically induced separator creep in lithium-ion battery capacity fade. Journal of Power Sources, 196(19), pp.8147-8153.

[12] Hua, X. and Gandee, E., 2021. Vibration and dynamics analysis of electric vehicle drivetrains. Journal of Low Frequency Noise, Vibration and Active Control, 40(3), pp.1241-1251.

[13] Yu, P., Zhang, T., Chen, S., Li, J. and Guo, R., 2015. Torsional Vibration Modeling of Driveline System for EV Low-Frequency Flutter (No. 2015-01-2191). SAE Technical Paper.